Combustion and Flame 254 (2023) 112854

Contents lists available at ScienceDirect

Combustion and Flame

journal homepage: www.elsevier.com/locate/combustflame

Prediction of knock intensity and validation in an optical SI engine

Jiabo Zhang[1], Hao Shi[1], Minh Bau Luong*, Qinglong Tang, Kalim Uddeen, Gaetano Magnotti, James Turner, Hong G. Im

Clean Combustion Research Center, King Abdullah University of Science and Technology, Thuwal, Saudi Arabia

ARTICLE INFO

Article history:
Received 19 January 2023
Revised 17 May 2023
Accepted 17 May 2023
Available online 26 May 2023

Keywords:
Knocking combustion
Knock intensity
Deflagration-to-detonation transition
Optical diagnostic
Computational prediction

ABSTRACT

To provide fundamental insights into the underlying mechanisms of knock occurrence in a spark-ignition (SI) engine, optical diagnostic measurements were performed at advanced spark timing under boosted conditions. Employing high-speed imaging, deflagration-to-detonation transition (DDT) processes were recorded. The states and locations of the unburned mixture more susceptible to autoignition were identified by statistically analyzing the recorded images of the spatial distribution of flame propagation and end-gas autoignition under distinct combustion modes. The relationships between the unburned mixture fraction (UMF) and two metrics associated with the knock intensity levels, namely the maximum amplitude of pressure oscillation (MAPO) and the peak in-cylinder pressure, P_{max}, were examined. In contrast to common beliefs, we found that the knock intensity represented by MAPO is not strongly correlated with UMF because UMF alone is inherently insufficient to represent the thermo-chemical properties of the bulk mixture inhomogeneities and its chemical reactivity at the onset of end-gas autoignition occurrence. Instead, a much stronger correlation was found between UMF and a newly proposed normalized-peak-pressure metric, allowing an *a prior* prediction of P_{max}, which is a critical parameter associated with the propensity of engine failure if P_{max} exceeds the strength limit of the engine. To quantitatively predict MAPO under SI-engine conditions, a refined model was proposed by imposing the pressure and temperature traces into the zero-dimensional (0-D) reactor model, such that the thermochemical properties of the *transient* mixture state at the onset of end-gas autoignition are properly incorporated into the predictive criteria. The model was validated against a large experimental dataset consisting of 619 cycles under various operating conditions. The results show that the model can reliably predict the end-gas autoignition and the knock intensity levels dictated by MAPO regardless of the stochastic nature of the knock development process.

1. Introduction

Towards higher efficiency, modern spark ignition (SI) engine designs have been adopting downsizing and boosting to achieve a high compression ratio [1]. However, operations at a high compression ratio are limited by the increased propensity of knock, defined as the end-gas autoignition, or super-knock, defined as the developing detonation process of reactant mixture prior to spark ignition [2]. For the boosted engine operation, super-knock is a serious concern due to its extreme pressure peaks and violent oscillations, potentially leading to severe mechanical damage. Therefore, an improved understanding of fundamental mechanisms of super-knock development is needed in order to develop a reliable predictive tool [3–7].

It is widely accepted that super-knock occurrence results from a resonance between the acoustic wave and the heat release in the end-gas region [8,9]. The coupling between chemical reactions and acoustic wave can accelerate the energy release of the unburned mixture, leading to more violent pressure spikes. As such, the super-knock cycles exhibit significant pressure rise and high knock intensity which can be dictated by the maximum in-cylinder pressure, P_{max}, and the maximum amplitude of pressure oscillation (MAPO) [10]. Specifically, P_{max} serves as an indicator for engine failure if P_{max} exceeds the engine strength limit, while the MAPO measures the amplitude of pressure fluctuation levels in the combustion chamber. Note that a high P_{max} may result either from (1) a high reactivity of the end-gas mixture state, i.e., high pressure and temperature near the top dead center (TDC) along with a large fraction of the remaining unburned mixture at the knock

* Corresponding author.
E-mail address: minhbau.luong@kaust.edu.sa (M.B. Luong).
[1] Authors have equal contribution.

https://doi.org/10.1016/j.combustflame.2023.112854
0010-2180/

onset (but not necessarily lead to a high MAPO); or from (2) a developing detonation process that also leads to extremely high MAPO due to pressure wave resonance [11]. In other words, P_{max} and MAPO are both useful quantities but may not be directly correlated.

In general, a higher level of unburned mixture fraction (UMF) at the onset of the end-gas autoignition is expected to yield a greater knock intensity level. To predict knock intensity, represented by MAPO, researchers have attempted to correlate it with UMF, but found a weak correlation between these two quantities due to the random nature of the phenomenon. For example, Wang et al. [12] reported that knock intensity increased with earlier preignition timing, higher UMF, and higher temperature/pressure of the unburned mixture, but no consistent correlation was found between knock intensity and any of the parameters. Zhou et al. [13] also studied the super-knock tendency in a SI engine, and found no clear relationship between knock intensity and knock onset for super-knock cases. Robert et al. [14] performed an analysis to predict knock intensity in relation to UMF at the knock onset. They also found that the correlations change significantly when shifting from a normal knocking cycle to a super-knocking cycle, and no unified metrics were found to reliably predict both normal knock and super-knock cases. These studies implied that the correlations between the unburned mixture and knock intensity are still largely unclear, which challenges the prediction of knock intensity, especially in super-knock cycles with excessive pressure oscillations and extremely high-pressure spikes. The lack of correlation between UMF and MAPO may be attributed to the differences in the thermochemical properties, the spatial non-uniformities, and reactivities of the unburned end-gas mixture at the knock onset [5–7,15,16]. These key parameters of the transient unburned mixture state need to be taken into consideration for a better prediction of combustion modes.

In contrast to using UMF as the key predictive metric, Bradley and coworkers [17,18] developed a detonation regime diagram that accounts for the spatial non-uniformity and reactivity of the hot spots which inherently exist in the unburned fuel/air mixture. The regime diagram employs two non-dimensional parameters, namely the *resonance parameter*, ξ, and the *reactivity parameter*, ε, to classify ignition regimes evolving from autoignitive hot spots. Kalghatgi et al. [2,19,20] effectively utilized the $\xi - \varepsilon$ regime diagram to distinguish different knocking cycles in a SI engine under various operation conditions. Specifically, the Livengood–Wu integral [21] was used to estimate the ignition delay time, τ_{ig}, and the resulting ξ and ε were then mapped into the regime diagram. The knocking cycles were reasonably identified by the detonation peninsula. However, the estimation of ξ and ε in the previous studies relied solely on the *initial* state of the mixture. Due to the stochastic nature of knocking cycles, knock intensity is found to depend largely on the *transient* thermo-chemical state of the unburned mixture just prior to the onset of end-gas autoignition [14,15]. As the unburned end-gas mixture generally undergoes a long transient duration due to the synergistic compression heating effect of the piston motion and propagating turbulence flames, a reliable prediction of normal/super-knock cycles requires an accurate representation of the transient mixture state prior to the onset of end-gas autoignition [5,16].

Recent studies have scrutinized the effects of the temporal evolution of the transient mixture state on detonation propensity [5–7,16,22,23]. For example, Pan et al. [24] numerically examined the effects of varied thermodynamic states caused by the reciprocating piston motion and the compression heating of the flame propagation on knock intensity in a SI engine, and quantitatively compared the differences in the corresponding detonation peninsula. Towery et al. [25] proposed a statistical model to evaluate the

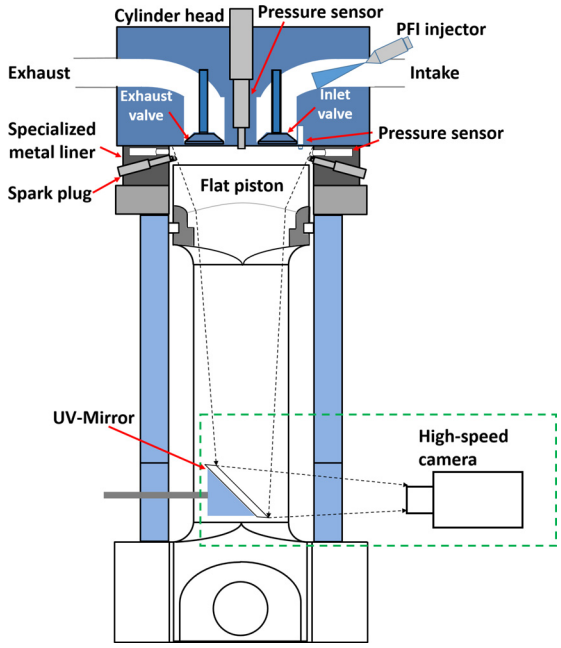

Fig. 1. Schematic diagram of the engine setup.

ξ and ε parameters in the presence of compressible isotropic turbulence fluctuations. The model can identify the developing detonation regime of an autoignitive gas resulting from turbulence-induced thermodynamic gradients. However, previous studies have not fully incorporated the transient end-gas mixture states of SI engines in evaluating the $\xi - \varepsilon$ parameters to improve a quantitative prediction of knock intensity covering normal/super-knock cycles [6,7,16].

To this end, the objective of this study is twofold: (1) to propose a new normalized metric for the correlation between the unburned mixture fraction and the peak in-cylinder pressure, (2) to develop a 0-D model that incorporates the transient state of unburned mixture of a SI engine to enable a better prediction of knock intensity levels. Optical diagnostics are conducted in a SI engine to visualize the developing detonation processes and to provide a large experimental dataset of the knocking cycles under various operating conditions in order to validate the predictive accuracy of the 0D model. The probability of the end-gas autoignition regions prone to the high knocking cycles is also statistically determined. A strong correlation between UMF and the ratio of the peak pressure to the pressure at the knock onset has been found for a wide range of engine conditions. The results indicate that the peak in-cylinder pressure and the knock intensity levels are well predicted by the newly developed criteria, as the thermo-chemical properties of the bulk mixture at the onset of end-gas autoignition are fully considered.

2. Experimental setup

2.1. Engine system

The experiments were implemented on a single-cylinder optical compression CI engine (AVL-5402). The engine was modified to operate under the SI mode of high knocking-intensity levels. The schematic diagram of the engine setup is shown in Fig. 1, and the engine specifications and operating conditions are listed in Table 1.

The original CI engine was modified to operate under the SI mode with port fuel injection (PFI). An inlet manifold was installed with a customized PFI module equipped with a port injector (SCRE 5405, Bosch). A customized metal liner was installed with four

Table 1
Engine specifications and operating conditions.

Description	Specifications
Stroke	90 mm
Bore	85 mm
Engine speed	1200 rpm
Compression ratio	9
Intake pressure	1, 1.2 bar
Intake temperature	25 °C
Coolant temperature	90 °C
Oil temperature	90 °C
Injection pressure	6 bar
Injection timing	−330 °aTDC
Injection duration	6500 μs
Excess air ratio (λ)	1

Table 2
High-speed imaging specifications.

Description	Specifications
Camera type	SA-4, Photron
Frame rate	72,000 fps
Shutter speed	1/118, 000
Resolution	384 × 384
Exposure time	12 μs
Recorded images	600/cycle
Camera triggering time	same with sparking time

spark plugs (ER8EH, NGK) and four pressure sensors (GH15DK, AVL) circumferentially, allowing spark ignition and pressure measurement from different sides of the cylinder. As multiple spark plug strategy may result in more concentrated directions of in-cylinder pressure oscillations and lower knock intensity due to a faster flame propagation mode [26,27], a spark plug located between the intake and exhaust valves was solely utilized to initiate the engine knock. The top pressure sensor installed on the engine head was used to monitor the cylinder pressure. More details of the engine setup can be found in Ref. [10].

The injection timing, the injection duration, and the spark timing (ST) were controlled by the IAV FI2RE commander software. The current signals of the injector and ignition coil were monitored by the IndiCom module (IndiCom 2.4, AVL). The intake pressure was directly controlled by an air flow meter, which was monitored by the AVL PUMA system. A stoichiometric PRF80/air mixture was used to facilitate the knock development. PRF80 is a blend of primary reference fuels, i.e., 80% *iso*-octane and 20% *n*-heptane by volume.

2.2. High-speed natural flame luminosity (NFL) imaging

As schematically shown in Fig. 1, an elongated piston was attached to the flat quartz piston crown (Suprasil 2 Grade B), which was surrounded by a metal shell for protection, leaving a viewing window with a diameter of 70 mm. With a UV mirror placed below, most of the combustion chamber was captured from the side. A vacuum pump was installed to inhale the air from the engine crankcase, preventing the oil splash during the engine operation and keeping the mirror clean.

Table 2 lists the specifications of a high-speed camera, FASTCAM SA4 Photron, which was used to record the combustion processes in the cylinder. A 50 mm, f/1.4 BK7-glass lens was used for the camera. The synchronization between the engine and camera was achieved by sending out the TTL triggering signals from the Indicom system. Under each tested condition, the first 200 continuous-firing cycles were used to warm up the engine reaching the steady states, and the data from the next 200 consecutive-firing cycles were recorded. The frame rate was set at 72,000 frames per second (fps), with an exposure time of 12 μs at an engine speed of 1200 rpm. The pixel resolution of the camera was 192 × 192. 600 images were collected in each cycle, starting from the spark timing. The first 50 images of each cycle were averaged for image processing to compute the background noise, and followed by denoising the flame images. Next, the flame intensities of these images were amplified to show the combustion processes.

3. Modeling approach

As mentioned earlier, the $\xi - \varepsilon$ regime diagram is a potential matrix to predict knock intensity in IC engines [2,19]. However, the stochastic nature of super-knock development processes makes the prediction of their knock intensity levels uncertain [5–7,14,22,23], especially when the criteria are evaluated solely based on the initial condition of the bulk unburned mixture. In a real IC engine under highly-boosted conditions, the initial state of the mixture has already undergone significant changes of ongoing reactions resulting in radical build-up and heat release, and a noticeable temperature and pressure rise that altogether facilitate the end-gas autoignition and subsequent detonation development [6,7,28–30]. An accurate determination of the instantaneous state of the highly-reactive unburned mixture at knock onset under transient conditions can improve the prediction of knock intensity. Previous studies [5–7,16] found that embedding the non-ideal temporal evolution of pressure and temperature rise in evaluating the sensitivity of the ignition delay time with respect to temperature variation results in a better prediction of ignition modes in shock tubes and compression ignition engines. Inspired by that idea, this study employed a zero-dimensional (0-D) ignition model to estimate the transient states of the unburned end-gas mixture and associated quantities which are needed to compute the transient ξ_t and ε_t parameters.

3.1. Zero-dimensional ignition model under SI-engine conditions

The main framework of the 0-D model in this study is that the temporal evolution of the experimental fired pressure, P_{fire}, and the peak hot-spot temperature, T_{hs}, are imposed into the model such that the resulting ignition process of the fuel/air mixture can realistically replicate the autoignition process of the end-gas in the optical combustion chamber. Due to evaporative fuel cooling, wall heat loss, and incomplete mixing, the temperature field in the combustion chamber is naturally developed and thus inherently inhomogeneous. Regardless of the random distribution of many hot spots in the form of eddies, the inhomogeneous temperature field can be decomposed into many dissipation elements such that the characteristic length scale of these hot spots can be determined [7,31]. The temperature variation of these hot spots under engine conditions is as large as 100 K [2,19,29,31–40] as experimentally measured by Dec et al. [41]. The compression heating from the burned gas also induces an additional increase in the temperature and pressure of the unburned end-gas mixture.

To account for these effects, the peak temperature of hot spots, T_{hs}, in the combustion chamber is evaluated using the adiabatic compression assumption as follows:

$$P(T/P)^{\gamma} = \text{constant} \tag{1}$$

$$T_{hs}/(T_{start} + \Delta T) = (P_{fire}/P_{start})^{(1-1/\gamma)} \tag{2}$$

where γ of 1.31 is chosen for all the cycles as in Ref. [31]. T_{hs} is estimated with the comparison of the fired pressure and temperature at t_{start}, namely P_{start} and T_{start}. Specifically, T_{hs} at t_{start} is assumed to be higher than the fired averaged temperature in the combustion chamber by a magnitude, ΔT, of 80 K, as adopted in previous studies [2,19,31]. By imposing the fired pressure, P_{fire}, T_{hs} at following crank angles is computed.

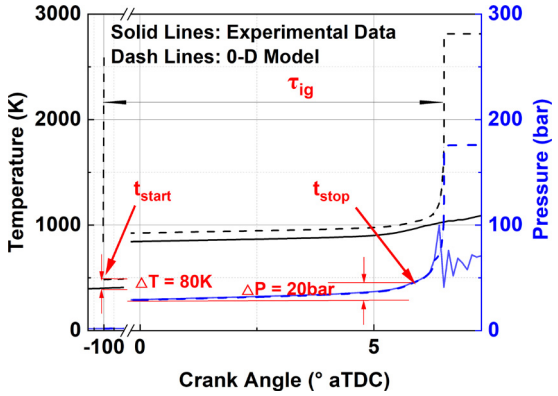

Fig. 2. Definition of the parameters used in the zero-dimensional (0-D) homogeneous-ignition model. t_{start} of −100 CAD aTDC and t_{stop} of 20 bar pressure increase from the spark timing are identified as the times to start and stop imposing the fired temperature and pressure into the 0-D model, respectively.

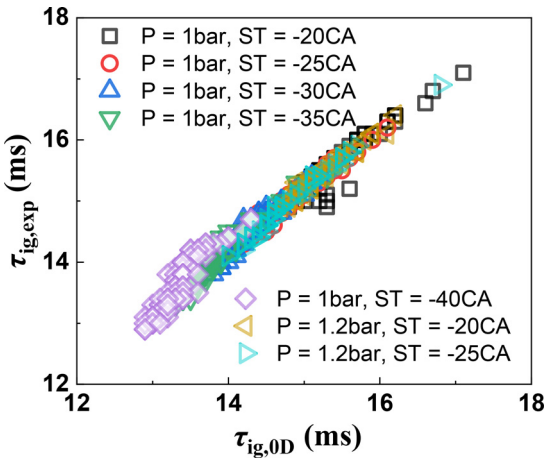

Fig. 3. Comparison between the predicted $\tau_{ig,0D}$ of the 0-D model and $\tau_{ig,exp}$ of experiments.

As schematically shown in Fig. 2, from t_{start} to t_{stop}, the fired pressure trace (blue solid line) and peak hot-spot temperature (black dash line) are imposed into the 0-D model, and afterwards the temperature and pressure rise of the 0-D model are driven solely by the thermochemical state of the system and by the motored compression and expansion induced by the reciprocating piston motion. The chemical kinetic mechanism developed by Liu et al. [42] is used to reproduce the homogeneous 0-D ignition delay time, $\tau_{ig,0D}$, of the PRF80/air mixture under IC-engine conditions. The corresponding sensitivity of $\tau_{ig,0D}$ to temperature variation, $\partial\tau_{ig,0D}/\partial T$, and the excitation time, τ_e, under realistic knocking conditions in SI engines are obtained simultaneously. Note that all 0-D simulations are started at t_{start} of -100 CAD aTDC from which the temporal pressure and temperature changes due to both reciprocating piston movement and kinetically released heat is fully emulated by the 0-D model [6,7,29]. As shown in Fig. 2, t_{stop} denotes the time instance at the onset of the main combustion process – the time at which the pressure increase approximately $\Delta P \approx 20$ bar as compared with the pressure at the spark timing. Note that $\Delta P \approx 20$ bar is chosen to ensure the accuracy of the proposed model in predicting the ignition delay time and to acquire the thermodynamic state of the *transient* mixture at the onset of the end-gas autoignition.

To validate the accuracy of the proposed 0-D model, the modelled ignition delay time, $\tau_{ig,0D}$, is compared with the experimental results, $\tau_{ig,exp}$. Note that the time interval between t_{start} and the time at which the modelled/measured temperature reaches its peak value is defined as the ignition delay time herein. A good agreement between $\tau_{ig,0D}$ and $\tau_{ig,exp}$ is obtained as readily seen in Fig. 3, verifying the fidelity of the 0-D model.

3.2. Computation of the transient ξ_t and ε_t numbers

Consistent with the original definition of the $\xi - \varepsilon$ numbers by Bradley and Gu [17,18], the transient ξ_t and ε_t numbers are defined as

$$\xi_t = \frac{a_t}{S_{sp}} = a_t / \left|\nabla \tau_{ig}\right|^{-1} = a_t \frac{\partial \tau_{ig,0D}}{\partial T}\frac{\partial T}{\partial x} \tag{3}$$

$$\varepsilon_t = (r_{hs}/a_t)/\tau_e \tag{4}$$

where ξ_t is defined as the ratio of transient sound speed, a_t, to the speed of the spontaneous ignition front, S_{sp}, which is determined by the spatial gradient of $\tau_{ig,0D}$. ε_t is defined as the ratio of the residence time, r_{hs}/a_t, of the acoustic wave within the hot spot with a radius, r_{hs}, to the excitation time, τ_e, in which most of the chemical energy is released. τ_e, $\tau_{ig,0D}$, and $\partial\tau_{ig,0D}/\partial T$ are computed using the 0-D model, and a_t is evaluated based on the *transient* mixture thermodynamic state at t_{stop}.

r_{hs} and $\partial T/\partial x$ are the length scale and the temperature gradient, respectively, of the hot spots, that represent the properties of the bulk mixture at the knock onset. Under the SI engine conditions in this study, r_{hs} is approximately 2 mm, which is half of the integral length scale [5,43–45], while $\partial T/\partial x$ of 2 K/mm is set as in the previous studies [2,19,46–48]. These two parameters were found to vary slightly with different engine conditions [2,19,31,46], and therefore are kept constant for all the engine cycles. Note that, although the choice of r_{hs}, and $\partial T/\partial x$ could quantitatively affect the absolute threshold values of ξ_t and ε_t, the overall trends and main conclusion remain the same in the following discussion.

3.3. Computation of the predictive ε_p number

In the $\xi - \varepsilon$ regime diagram [17,18], a typical C-shaped detonation peninsula is bounded by the upper and lower ξ limits, $\xi_{u,l} \sim 1 - \mathcal{O}(10)$, and the left boundary of ε, $\varepsilon > \varepsilon_m$. However, there is no well-defined threshold value of ε_m, i.e., ε_m was found to vary case by case being system-dependent. By recognizing this limitation, Luong and Im [7] developed a predictive ε_p number that can effectively identify the leftmost boundary of the C-shaped detonation peninsula:

$$\varepsilon_p = r_{hs}/\ (l_m/\alpha) \tag{5}$$

where l_m is the minimum run-up distance of direct detonation initiation by an autoignitive hot spot [6]; α is a weighting factor that accounts for the multi-dimensional effect of the interaction and collision of multiple ignition fronts in the highly-reactive transient mixture conditions. As quantitatively observed in recent multi-dimensional direct numerical simulation (DNS) studies [4–7], the interaction and collision of the multiple ignition kernels promote the onset of localized detonation development, shortening the run-up distance requirement for detonation by approximately a factor (α) of 4. Note that a similar definition of ε_p was introduced in Ref. [25], but the transient instantaneous state of the reactant mixture and the α factor were not considered in that study.

The magnitude of l_m is determined through its strong linear correlation with the exothermic characteristic length scale, l_{exo}. The correlation between l_m and l_{exo} found in the previous one-dimensional simulations [6] was validated for fuels with and without negative temperature coefficient (NTC) behavior over a wide range of constant-volume and IC-engine conditions. The exothermic characteristic length scale is defined as $l_{exo} = a_t \tau_{exo}$ where a_t

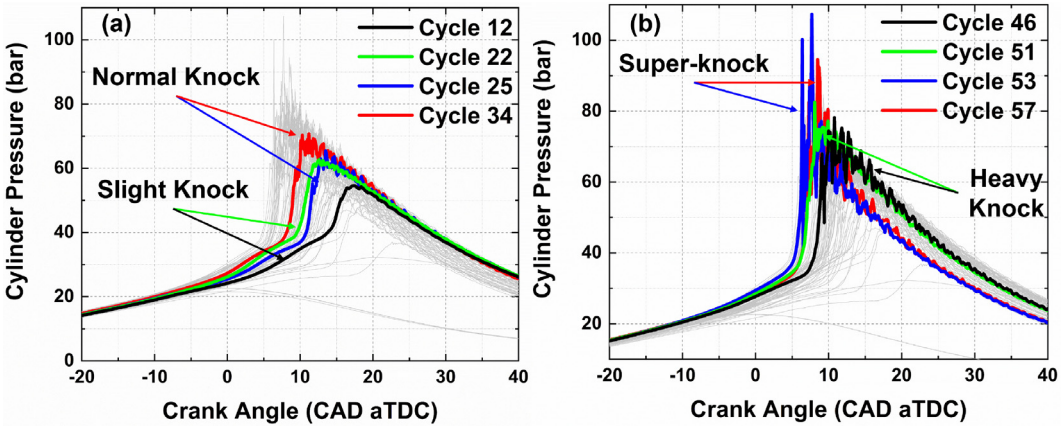

Fig. 4. Pressure traces of 70 representative knocking cycles (gray color) at P_{in} = 1.2 bar and ST = −20 CAD aTDC: (a) slight knock and normal knock, (b) heavy knock and super-knock.

is the transient sound speed, and τ_{exo} is the exothermic time scale. The transient mixture state at the knock onset extracted from the 0-D model is taken as the initial condition to the ideal Zeldovich, Doering, and von Neumann (ZND) detonation model to compute τ_{exo}. τ_{exo} is defined as the time interval between the time that HRR first increases to 50% of its peak HRR and the time HRR first decreases to 50% of its peak HRR.

The significance of ε_p is that no detonation is expected for $\varepsilon_p \ll 1$ regardless of the magnitude of ξ_t due mainly to a too small hot-spot size and/or a too slow/fast chemical time scale that do not promote the mutual coupling between the pressure wave and HRR for detonation initiation. As ε_p approaches unity, the transient mixture state shifts towards the boundary of the detonation peninsula, and the developing detonation is expected, resulting in strong pressure oscillations and high-pressure spikes. For $\varepsilon_p \gg 1$, fully developed detonation is expected to occur for $\xi_t \sim O(1)$ to $O(10)$. A direct comparison between the ε_t and ε_p on the prediction of knock intensity will be examined in the next section.

4. Results and discussion

4.1. Overall combustion characteristics

We conducted experiments under various engine operating conditions of varied intake pressure and sparking timing, and collected a total number of 619 cycles exhibiting different levels of knocking intensity to analyze their combustion characteristics. As a representative example, the pressure traces of 70 knocking cycles at boosted intake pressure of 1.2 bar and advance sparking timing of −20 °CA are shown in Fig. 4. Among these 70 knocking cycles, eight typical cycles exhibiting distinct levels of knock intensity are chosen for further analysis of the maximum amplitude of pressure oscillation (MAPO).

These eight sampling cycles are representative of four different knocking levels, ranging from slight knock to super-knock. Particularly, the knocking-intensity level gradually increases from slight knock (cycles 12 and 22), to normal knock (cycles 25 and 34), heavy knock (cycles 46 and 51), and super-knock (cycles 53 and 57). As readily seen in Fig. 4(b), the cycle 53 in blue exhibits the most severe pressure oscillations as depicted by MAPO of 39.86 bar, and the highest peak pressure of 108.2 bar. The knock onset of the cycle 53 occurs at −1.5 °CA aTDC, which is closest to the TDC as compared to other knocking cycles. Under such a favorable condition of the highest temperature and pressure, and a large amount of the remaining highly-reactive unburned mixture at the knock onset, the end-gas autoignition process of this cycle is more prone to detonation development than other cycles.

4.2. Optical diagnostics on knocking combustion processes of the sampled cycles

To reveal the end-gas autoignition process, the high-speed imaging of these knocking cycles is analyzed. Figs. 5 and 6 show the evolution of flame propagation and end-gas autoignition process for the sampled cycles. To visualize the knocking combustion processes of these cycles exhibiting different knock strength levels and peak pressure, a series of amplification factors of flame intensity (listed in the lower right corner) were applied. Note that due to the constraints on the knock intensity limit of the optical engine, strong detonation cases were not conducted in this study. However, several DDT cycles are still observed, i.e., in cycles 53 and 57 in Fig. 6. Several points are made from these figures.

For the mild knock intensity cycles (cycles 12, 22, 25 and 34 in Fig. 4), their end-gas autoignition process are difficult to detect by the integrated signal. Taking cycle 25 in Fig. 5 as an example for normal knock, the initial autoignition area is visualized at 10 CAD aTDC, and the spark-initiated flame consumes nearly half of the air/fuel mixture. Two emerging autoignition kernels are observed at 10.4 and 11 CAD aTDC. Due to the low UMF of this cycle, the flame intensity fluctuations resulting from knock are nearly homogeneous, confirming a mild knock intensity level.

Unlike the mild knock cases, the autoignition of the heavy knock cases can be readily detected at earlier time. Particularly, the first autoignition kernel in cycle 51 (see Fig. 6) emerges at 5.1 CAD aTDC. Multiple autoignition spots then emanate in a very short period of time that further aggravates the knock strength.

For the DDT process of the cycle 53, its autoignition initiates approximately at -1.5 CAD aTDC. At 5.5 CAD aTDC, many noticeable auto-ignited kernels emerge in the combustion chamber, quickly consuming a large amount of UMF and resulting in a short ignition delay time in this cycle. At 6.1 CAD aTDC, a large cylinder area is dominated by the autoignition, facilitating the DDT process in the end-gas. The shock wave emerges from the right side of the cylinder at 6.2 CAD aTDC, and it propagates rapidly towards the opposite side as marked by the red arrows. At 6.3 CAD aTDC, the speed of the developing detonation front reaching the cylinder center is approximately 1440 m/s, which is much higher than the local sound speed. As the detonation wave front reaches the end-wall, its propagation speed accelerates quickly from 1440 m/s to 3060 m/s. This value is approximately 1.5 times higher than the CJ velocity, implying that the DDT is likely to occur in this cycle. It is

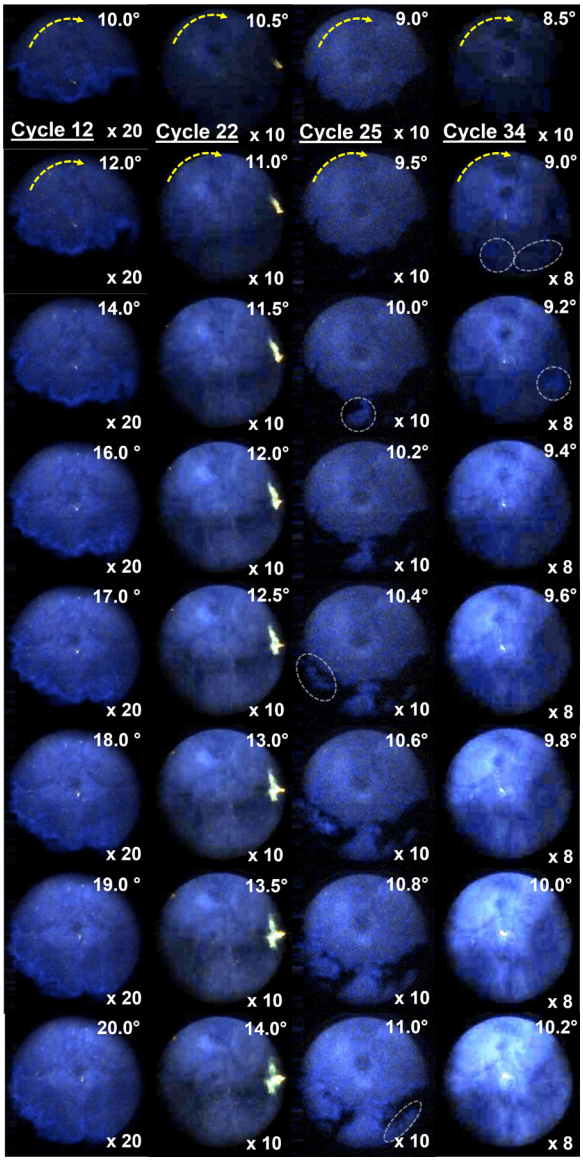

Fig. 5. Knocking combustion processes in sampling cycles: normal knock (cycles 12 and 22) and mild knock (cycles 25 and 34) at P_{in} = 1.2 bar and ST = −20 CAD aTDC. The corresponding crank angle of each image is marked in the upper-right corner in each image. The white dashed circles mark the emerged autoignition kernels during the knocking combustion processes. The yellow arrows in the first two images of each cycle indicate the swirl direction. (For interpretation of the references to color in this figure legend, the reader is referred to the web version of this article.)

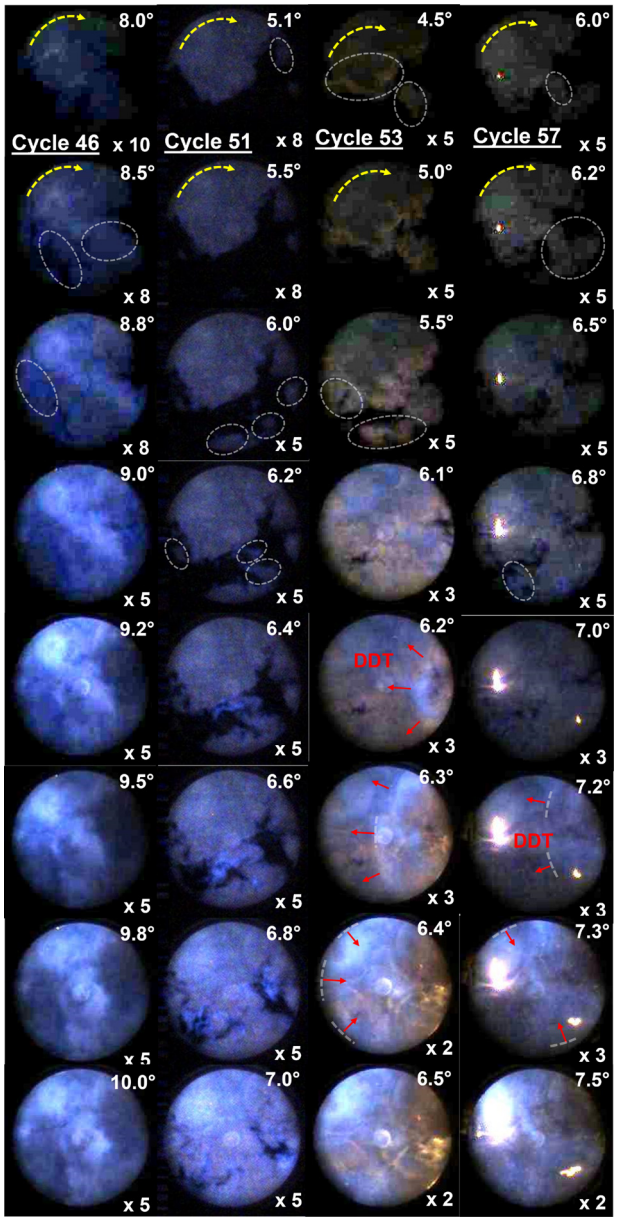

Fig. 6. Knocking combustion processes in sampling cycles: heavy knock (cycles 46 and 51) and super knock (cycles 53 and 57) at P_{in} = 1.2 bar and ST = −20 CAD aTDC. The corresponding crank angle of each image is marked in the upper-right corner in each image. The white dashed circles mark the emerged autoignition kernels during the knocking combustion processes. The shock waves and their spreading directions are marked with white curves and red arrows, respectively. The yellow arrows in the first two images of each cycle indicate the swirl direction. (For interpretation of the references to color in this figure legend, the reader is referred to the web version of this article.)

also seen that the UMF area is largely consumed by the DDT process, i.e., constituting nearly half of the entire combustion chamber. The detonation waves reflecting back and forth consuming the remaining UMF lead to violent pressure oscillations in the combustion chamber.

4.3. Identification of the probability of knocking regions in the combustion chamber

All the recorded images are processed to quantitatively determine the remaining UMF prior to the end-gas autoignition, and to statistically identify the regions in the combustion chamber that are prone to the end-gas autoignition. Note that there may be a general tendency that a higher level of UMF would increase the reactivity of the hot spots in the end gas region; however, the UMF is not directly related to the generation of temperature field (hot spots). The hot spots are inherently present in the end gas bulk mixture. For example, the temperature fluctuation, T', measured at the top dead center (TDC) in an SI engine is approximately 10 K [49]. Even in an HCCI engine, T' of up to 13.3 K was observed at TDC [50]. These temperature fluctuations are randomly distributed by turbulent eddies, and the corresponding length scale and gradient level can be statistically determined as an averaged quantity of the bulk mixture [7].

The extracted UMF distribution of the sampled cycles are shown in Fig. 7. Different curves are used in Fig. 7(a) to discern the cylinder wall (black), and autoignition boundaries of cycle 25 (blue), cycle 51 (pink) and cycle 53 (red). In particular, the cyan

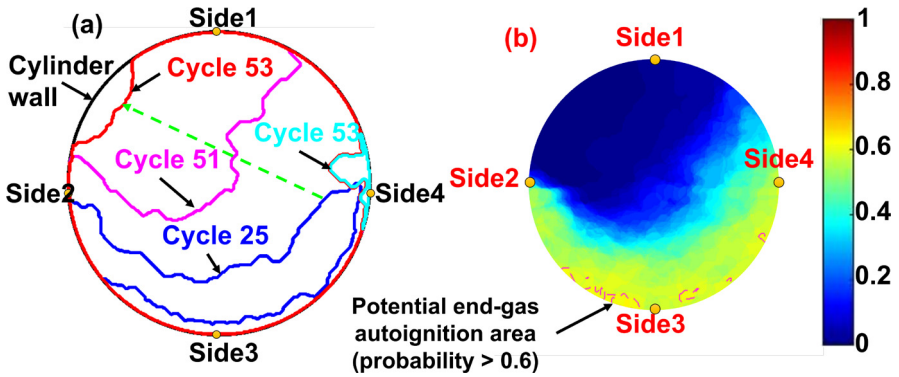

Fig. 7. Statistical results of (a) autoignition and detonation areas of the sampled cycles, and (b) the probability of the end-gas autoignition distribution.

curve denotes the boundary of initial developing detonation area in cycle 53. Although the initial autoignition spot is unpredictable due to the knock randomness and cycle-to-cycle variations, most of the autoignition kernels originate from the lower part of the cylinder area while the flame initiated at the Side 2 propagates clockwise due to the swirl effect (see Figs. 5 and 6).

As extracted from Fig. 7(a), less than 30% of the cylinder area is covered by autoignition in cycle 25 while it takes up more than 60% of the entire cylinder area in cycle 51. In the cycle 53, the autoignition initiates at a much earlier time, hence an approximate 90% UMF still remains. As a result, multiple ignition kernels occur simultaneously throughout the combustion chamber (see Fig. 6 at 4.5–5.5 CAD aTDC), causing a steep pressure rise and high-frequency fluctuations. As seen in Fig. 6, the spontaneous ignition fronts occur at multiple locations, generating a rapid heat release, and thus making the in-cylinder pressure rise considerably, i.e., the peak pressure of the cycle 53 exceeds 100 bar. The underlying mechanism of super-knock development in the cycle 53 is the coherent coupling between the volumetric heat release of the unburned mixture reactions and pressure waves that reinforces the development of the initial shock waves in the end-gas region (cyan curve in Fig. 7(a)), and hence promotes detonation development.

The probability of the end-gas autoignition for all the knocking cycles is statistically computed and shown in Fig. 7(b). To obtain the probability, the flame boundaries for all knocking cycles are first identified and located employing synchronized high-speed imaging. Subsequently, the end-gas regions are split from the main flame, and the distribution probability of end-gas autoignition in the combustion chamber is calculated by averaging all cycle data. More details can be found in our previous work [10]. The result reveals that the end-gas zone is mostly distributed in the lower part close to Side 3, taking up approximately one third of the entire cylinder area. This is attributed to the clock-wise flame propagation in the cylinder. In addition, the fuel/air mixture in the upper part, lying between Side 2, Side 1, and Side 4, is mostly consumed by the flame initiated by the spark ignition as depicted by a low probability of the end-gas autoignition in this region. In contrast, the area with high probability of the end-gas autoignition distribution, i.e., probability > 0.6, is highlighted and can be seen near the wall lying between Side 4, Side 3, and Side 2.

The results suggest that higher UMF remains at the knock onset tends to enhance the knock intensity. The relationship between the UMF at knock onset and knock intensity is analyzed in the next section.

4.4. Relationship between the unburned mixture and knock intensity

Unlike the correlation between UMF and a dimension parameter MAPO which has been widely adopted in many previous studies, in this study, we propose the correlation between UMF and the normalized peak pressure, P_{max}/P_{ign} where P_{max} and P_{ign} denote the maximum (peak) cylinder pressure, and the pressure at the knock onset, respectively. The significance of P_{max}/P_{ign} is that the *transient* thermodynamic state of the unburned mixture is simultaneously considered in the relationship between the unburned mixture and knock intensity. For a direct comparison between these two correlations, Figs. 8 and 9 show the MAPO and normalized peak pressure, P_{max}/P_{ign}, respectively, as a function of UMF for all the knocking cycles. Note that a method that relies on a band-pass filtered

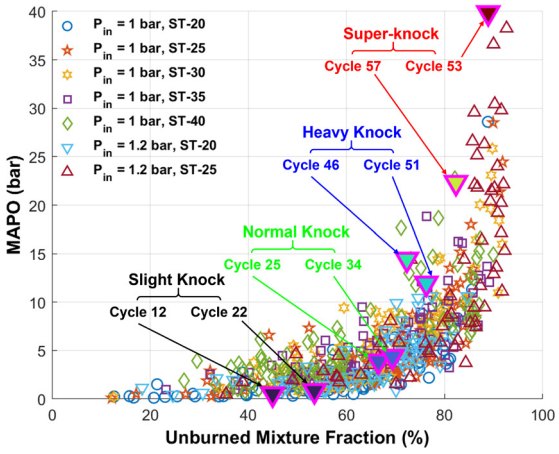

Fig. 8. The correlation between UMF and MAPO.

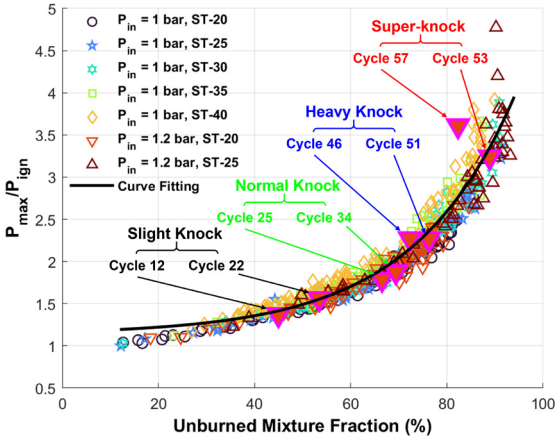

Fig. 9. The correlation between UMF and the normalized peak pressure, P_{max}/P_{ign}. The correlation curve in black is approximated by a function fitting, $y = 1.134 + 0.034e^{0.047x}$.

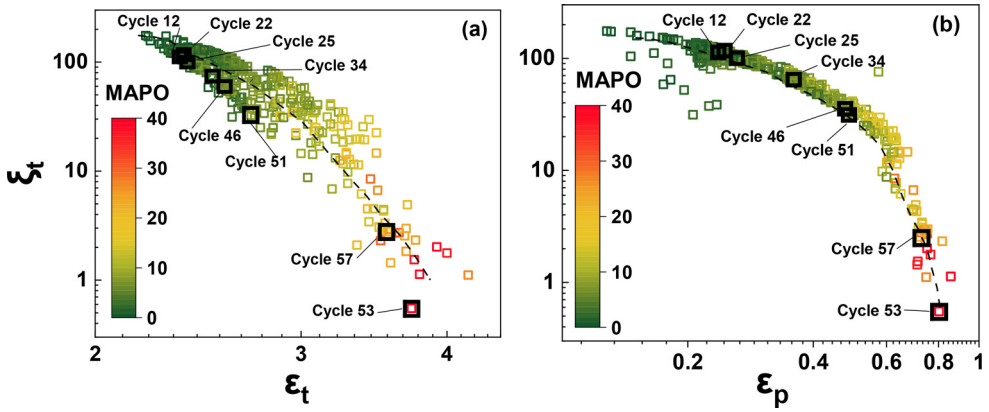

Fig. 10. MAPO of all the 619 engine cycles in (a) the $\xi_t - \varepsilon_t$ regime diagram, and in (b) the $\xi_t - \varepsilon_p$ regime diagram.

pressure with a pressure threshold of 0.1 bar is used to determine the knock onset [26]. This method was validated by a large dataset obtained from the synchronized high-speed imaging. More details of this method can be found in Ref. [10].

As seen in Figs. 8 and 9, in general, both MAPO and normalized peak pressure increase proportionally with increasing UMF, indicating that the cycle with a higher proportion of unburned fuel/air mixture at the knock onset has a higher propensity to experience a stronger knock intensity level. Unlike a widely-scattered weak correlation between UMF and MAPO shown in Fig. 8 making the MAPO-based knock intensity level vary considerably at the same UMF, Fig. 9 shows a strong correlation between the normalized peak pressure and UMF. This strong correlation is attributed to the full consideration of the *transient* mixture state at the onset of end-gas autoignition in the normalized peak pressure. With the normalization of P_{ign}, the effects of variations in initial thermodynamic conditions at end-gas autoignition due to the stochastic nature of knock occurrence are reduced, leading to a more consistent representation of the knock intensity level for a given UMF. Moreover, this good correlation can be approximated by a function fitting, $y = 1.134 + 0.034e^{0.047x}$ with the R-squared value is 0.935. Given UMF and the pressure at the knock onset, this exponential function can be used to determine *a priori* the peak pressure.

In this study, the effect of the swirl variation on the hot spot generation and the knock intensity is not studied. It was reported that proper design and tuning of moderate swirl result in a more uniform distribution of temperature, reducing the likelihood of localized hot spots and mitigating knock [51]. In contrast, excessive swirl may spread the temperature nonuniformity to a broader area, leading to n enhancement of detonation run-up distance, thus promoting the knock propensity [40,52].

4.5. Identification of knock intensity levels in the detonation regime diagram

In this section, with the help of the 0-D model, all 619 engine cycles are mapped into the detonation regime diagram to identify the developing detonation regime, and also to verify the accuracy of the predictive criteria. Note that, as UMF alone is insufficient to describe the end-gas state, the 0-D model incorporates the information of the temporal evolution of the end gas mixture, including the hot spot size and its gradient level, into the predictive criteria. A direct side-by-side comparison between ε_t and ε_p criteria plotted in the $\xi_t - \varepsilon_t$ regime diagram and the $\xi_t - \varepsilon_p$ regime diagram is shown in Figs. 10 and 11, where data points are colored by MAPO and the normalized peak pressure, P_{max}/P_{ign}, respectively, to identify the developing detonation regime [13,26,53]. Three main points are made from these figures.

First, both $\xi_t - \varepsilon_t$ and $\xi_t - \varepsilon_p$ diagrams can identify the overall trajectory of developing knock intensity levels of consecutive cycles. Consistent with the overall trend of MAPO in the detonation regime diagram, P_{max}/P_{ign} monotonically increases with decreasing ξ_t and increasing ε_t or ε_p. In particular, knock intensity shifts from weak knock (cycles 12 to cycles 25), to heavy knock (cycles 34 to cycles 51), and super-knock (cycles 53 and 57).

Second, as shown in Fig. 10, the cycles with high magnitudes of MAPO are well captured in the region of $\xi_t \sim \mathcal{O}(1)$. In the vicinity of the detonation peninsula, the amplitude of the pressure oscillations characterized by MAPO increases significantly due to the reinforced coupling between the pressure wave and rapid chemical energy release. The transient $\xi_t \sim \mathcal{O}(1)$ found in this study for many high-knocking intensity cycles is consistent with the observation from Dai et al. [22], who computed the averaged ξ of the transient evolution of the hot spots, and found that the C-shaped detonation peninsula is bounded by the upper and lower ξ limits, $\xi_{u,l} \sim 0.5 - 2.5$, regardless of the initial conditions.

In contrast to MAPO, the cycles with high values of P_{max}/P_{ign} in Fig. 11 are scattered over a wider range of ξ_t, making it difficult in distinguishing the developing detonation regime. The strong correlation between P_{max}/P_{ign} and UMF shown in Fig. 9 along with the result in Fig. 11 verify that UMF and P_{max}/P_{ign} are not an effective metric to characterize the amplitude of the pressure oscillations. However, the strong correlation between P_{max}/P_{ign} and UMF does enable an *a priori* prediction of P_{max} which is a critical parameter informing the possibility of the engine failure if P_{max} exceeds a certain threshold.

Third, the threshold value, ε_p of 1, is demonstrated to effectively identify the leftmost boundary of the C-shaped detonation peninsula while there is no a well-defined threshold value ε_t to determine this boundary in the $\xi_t - \varepsilon_t$ diagram. In addition, the cycles exhibiting a comparable MAPO have a nearly-identical ε_p value while their corresponding ε_t is more widely distributed. As shown in Fig. 10(b), the super-knock cycles are consistently predicted by the ε_p number, $\varepsilon_p \sim O(1)$, indicating that all the super-knock cases located in the vicinity of the boundary of the developing detonation regime. In other words, as the magnitude of ε_p of these super-knock cycles approaches unity, shifting them towards the boundary of the detonation peninsula, and thus the developing detonation is likely to occur. As a result, these cycles experience strong pressure oscillations and high-pressure spikes, but no strong direct detonation initiation is expected as confirmed by their P_{max} that is much lower than the detonation pressure spike, $P_{max} \ll P_{VN}$. Note that no strong detonation cases were conducted in the optical engine due to the limit of its structure strength, confirming that the computed ε_p values are completely consistent with the knock intensity levels measured in the experiments.

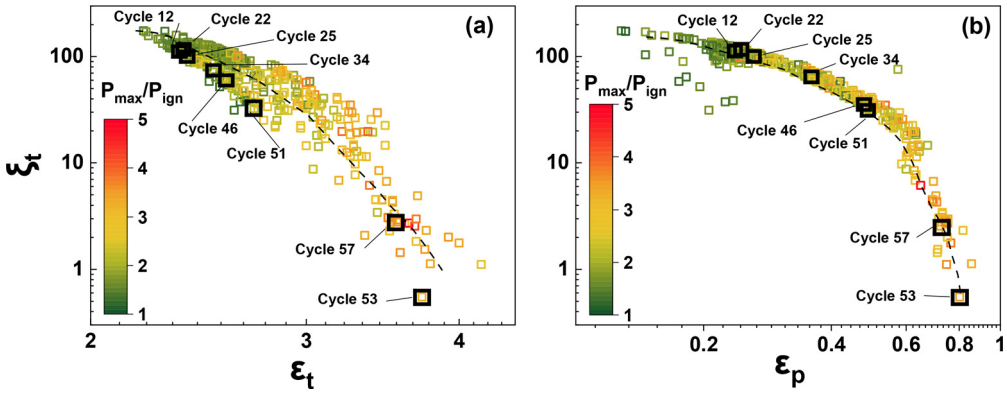

Fig. 11. The normalized peak pressure of all the 619 engine cycles in (a) the $\xi_t - \varepsilon_t$ regime diagram, and in (b) the $\xi_t - \varepsilon_p$ regime diagram.

As a final remark, the prediction of the model proposed in this study is not entirely predictive since it relies on the temporal evolution of the fired pressure trace. However, the experimental results in this study reveal that the engine cycles are more likely to undergo many mild knocking cycles prior to transiting into a more severe knocking cycle. As a result, the trajectory history of super-knock evolution can be well captured by the $\xi_t - \varepsilon_p$ regime diagram, shifting from the mild knock regime into the developing detonation regime. Thanks to the good correlation with knock intensity levels measured by MAPO, if sequential cycles that exhibit developing knock-intensity levels are well-predicted by the $\xi_t - \varepsilon_p$ parameters, the engine control unit (ECU) can take necessary actions to suppress the potential development of super-knock cycles.

5. Conclusions

In this work, optical diagnostics were implemented to investigate the knock phenomena of a PRF80-fueled SI engine under various spark timing and intake pressure conditions. The combustion processes of various knocking cycles were recorded using a 72 kHz high-speed imaging system. The knock intensities characterized by either the maximum amplitude of pressure oscillation (MAPO) or the peak in-cylinder pressure, $P_{\max}$, were correlated with the detected unburned mixture fraction (UMF). A 0-D model was also developed to extract the transient thermo-chemical state of the in-cylinder mixture prior to the combustion onset which allows a better prediction of combustion modes and knock intensity levels in the SI engine. Some key conclusions in this study are listed as follows:

(1) Typical deflagration-to-detonation transition (DDT) cycles were visualized at boost and advanced spark timing conditions. These cycles had earlier knock onsets with UMFs close to 90%, making the end-gas autoignition process of the bulk gas in these cycles most severe, and thereby resulting in the largest MAPO and the maximum peak pressure. Destructive shock waves reflecting back and forth to the combustion chamber wall were observed in the end-gas. Their propagation speeds is comparable with the CJ speed.

(2) The relationship between the UMF at knock onset and knock intensity was also examined. In particular, UMF was found to be weakly correlated with MAPO, as UMF alone is inherently insufficient to represent the stochastic nature of knock occurrence. In contrast, a strong correlation between UMF and the normalized pressure, $P_{\max}/P_{ign}$, was found, which is primarily because the detailed information on the spatial-temporal non-uniformity and reactivity of the *transient* thermo-chemical states of the highly-reactive end-gas bulk mixtures at the autoignition occurrence is fully considered. The good correlation between $P_{\max}/P_{ign}$ and UMF allows an *a priori* prediction of the peak in-cylinder pressure.

(3) By incorporating the fired temperature and pressure traces into a 0-D model, the *transient* thermo-chemical states of the end-gas prior to the main combustion were obtained, leading to a more accurate determination of the ξ_t, ε_t, and ε_p parameters for knock intensity predictions. Both the $\xi_t - \varepsilon_t$ and $\xi_t - \varepsilon_p$ diagram can reliably predict the knock intensity, particularly that represented by MAPO, and the results showed a consistent agreement with the experimental data.

Declaration of Competing Interest

The authors declare that they have no known competing financial interests or personal relationships that could have appeared to influence the work reported in this paper.

Acknowledgement

This work was sponsored by competitive research funding (URF/1/3710-01-01) from the King Abdullah University of Science and Technology (KAUST) and used the resources of the KAUST Supercomputing Laboratory (KSL).

References

[1] T. Inoue, Y. Inoue, M. Ishikawa, Abnormal Combustion in a Highly Boosted SI Engine-the Occurrence of Super Knock, Technical Report, SAE Tech. Paper, 2012.
[2] G.T. Kalghatgi, D. Bradley, Pre-ignition and 'super-knock' in turbo-charged spark-ignition engines, Int. J. Engine Res. 13 (4) (2012) 399–414.
[3] M.B. Luong, F.E. Hernández Pérez, H.G. Im, Prediction of ignition modes of NTC-fuel/air mixtures with temperature and concentration fluctuations, Combust. Flame 213 (2020) 382–393.
[4] M.B. Luong, S. Desai, F.E.H. Pérez, R. Sankaran, B. Johansson, H.G. Im, A statistical analysis of developing knock intensity in a mixture with temperature inhomogeneities, Proc. Combust. Inst. 38 (4) (2021) 5781–5789.
[5] M.B. Luong, H.G. Im, Direct numerical simulation of preignition and knock in engine conditions, Advances in Energy and Combustion, Springer (2022), pp. 311–336.
[6] M.B. Luong, H.G. Im, Effects of low-temperature chemistry on the direct detonation initiation by a hot spot under engine conditions, Proc. Combust. Inst. (2022), doi:10.1016/j.proci.2022.11.008.
[7] M.B. Luong, H.G. Im, Prediction of the developing detonation in an NTC-fuel/air mixture with temperature inhomogeneities under engine conditions, Proc. Combust. Inst. (2022), doi:10.1016/j.proci.2022.10.015.
[8] H. Yu, Z. Chen, End-gas autoignition and detonation development in a closed chamber, Combust. Flame 162 (11) (2015) 4102–4111.
[9] M.B. Luong, G.H. Yu, S.H. Chung, C.S. Yoo, Ignition of a lean prf/air mixture under RCCI/SCCI conditions: chemical aspects, Proc. Combust. Inst. 36 (2017) 3587–3596.
[10] H. Shi, Q. Tang, K. Uddeen, G. Magnotti, J. Turner, Optical diagnostics and multi-point pressure sensing on the knocking combustion with multiple spark ignition, Combust. Flame 236 (2022) 111802.
[11] Z. Wang, H. Liu, R.D. Reitz, Knocking combustion in spark-ignition engines, Prog. Energy Combust. Sci. 61 (2017) 78–112.

[12] Z. Wang, H. Liu, T. Song, Y. Qi, X. He, S. Shuai, J. Wang, Relationship between super-knock and pre-ignition, Int. J. Engine Res. 16 (2) (2015) 166–180.
[13] L. Zhou, R. Kang, H. Wei, D. Feng, J. Hua, J. Pan, R. Chen, Experimental analysis of super-knock occurrence based on a spark ignition engine with high compression ratio, Energy 165 (2018) 68–75.
[14] A. Robert, S. Richard, O. Colin, T. Poinsot, LES study of deflagration to detonation mechanisms in a downsized spark ignition engine, Combust. Flame 162 (7) (2015) 2788–2807.
[15] Y. Qi, Z. Wang, J. Wang, X. He, Effects of thermodynamic conditions on the end gas combustion mode associated with engine knock, Combust. Flame 162 (11) (2015) 4119–4128.
[16] M. Figueroa-Labastida, M.B. Luong, J. Badra, H.G. Im, A. Farooq, Experimental and computational studies of methanol and ethanolpreignition behind reflected shock waves, Combust. Flame 234 (2021) 111621.
[17] X. Gu, D. Emerson, D. Bradley, Modes of reaction front propagation from hot spots, Combust. Flame 133 (1–2) (2003) 63–74.
[18] D. Bradley, C. Morley, X. Gu, D. Emerson, Amplified pressure waves during autoignition: relevance to CAI engines, SAE Trans. paper (2002) 2679–2690.
[19] G. Kalghatgi, I. Algunaibet, K. Morganti, On knock intensity and superknock in SI engines, SAE Int. J. Engines 10 (3) (2017) 1051–1063.
[20] D. Bradley, G.T. Kalghatgi, Influence of autoignition delay time characteristics of different fuels on pressure waves and knock in reciprocating engines, Combust. Flame 156 (12) (2009) 2307–2318.
[21] J. Livengood, et al., Correlation of autoignition phenomena in internal combustion engines and rapid compression machines, Symp. (Int.) Combust. 5 (1955) 347–356.
[22] P. Dai, Z. Chen, Effects of NOx addition on autoignition and detonation development in DME/air under engine-relevant conditions, Proc. Combust. Inst. 37 (4) (2019) 4813–4820.
[23] J. Pan, H. Wei, G. Shu, Z. Chen, P. Zhao, The role of low temperature chemistry in combustion mode development under elevated pressures, Combust. Flame 174 (2016) 179–193.
[24] J. Pan, L. Chen, H. Wei, D. Feng, S. Deng, G. Shu, On autoignition mode under variable thermodynamic state of internal combustion engines, Int. J. Engine Res. 21 (5) (2020) 856–865.
[25] C.A. Towery, A.Y. Poludnenko, P.E. Hamlington, Detonation initiation by compressible turbulence thermodynamic fluctuations, Combust. Flame 213 (2020) 172–183.
[26] H. Shi, K. Uddeen, Y. An, Y. Pei, B. Johansson, Statistical study on engine knock oscillation and heat release using multiple spark plugs and pressure sensors, Fuel 297 (2021) 120746.
[27] H. Shi, K. Uddeen, Y. An, Y. Pei, B. Johansson, Multiple spark plugs coupled with pressure sensors: anew approach for knock mechanism study on SI engines, Energy 227 (2021) 120382.
[28] M.B. Luong, G.H. Yu, T. Lu, S.H. Chung, C.S. Yoo, Direct numerical simulations of ignition of a lean *n*-heptane/air mixture with temperature and composition inhomogeneities relevant to HCCI and SCCI combustion, Combust. Flame 162 (2015) 4566–4585.
[29] M.B. Luong, R. Sankaran, G.H. Yu, S.H. Chung, C.S. Yoo, On the effect of injection timing on the ignition of lean PRF/air/EGR mixtures under direct dual fuel stratification conditions, Combust. Flame 183 (2017) 309–321.
[30] G.H. Yu, M.B. Luong, S.H. Chung, C.S. Yoo, Ignition characteristics of a temporally evolving *n*-heptane jet in an *iso*-octane/air stream under RCCI combustion-relevant conditions,, Combust. Flame 208 (2019) 299–312.
[31] N. Peters, B. Kerschgens, G. Paczko, Super-knock prediction using a refined theory of turbulence, SAE Int. J. Engines 6 (2) (2013) 953–967.
[32] M.B. Luong, Z. Luo, T. Lu, S.H. Chung, C.S. Yoo, Direct numerical simulations of the ignition of lean primary reference fuel/air mixtures with temperature inhomogeneities, Combust. Flame 160 (2013) 2038–2047.
[33] M.B. Luong, T. Lu, S.H. Chung, C.S. Yoo, Direct numerical simulations of the ignition of a lean biodiesel/air mixture with temperature and composition inhomogeneities at high pressure and intermediate temperature, Combust. Flame 161 (2014) 2878–2889.
[34] S.O. Kim, M.B. Luong, J.H. Chen, C.S. Yoo, A DNS study of the ignition of lean PRF/air mixtures with temperature inhomogeneities under high pressure and intermediate temperature, Combust. Flame 162 (2015) 717–726.
[35] M.B. Luong, G.H. Yu, S.H. Chung, C.S. Yoo, Ignition of a lean PRF/air mixture under RCCI/SCCI conditions: a comparative DNS study, Proc. Combust. Inst. 36 (2017) 3623–3631.
[36] M.B. Luong, G.H. Yu, S.H. Chung, C.S. Yoo, Ignition of a lean PRF/air mixture under RCCI/SCCI conditions: chemical aspects, Proc. Combust. Inst. 36 (2017) 3587–3596.
[37] M.B. Luong, F.E. Hernández Pérez, A. Sow, H.G. Im, Prediction of ignition regimes in DME/air mixtures with temperature and concentration fluctuations, AIAA SciTech 2019 Forum (2019). doi:10.2514/6.2019-2241.
[38] M.J.M. Ali, M.B. Luong, A. Sow, F.E. Hernández Pérez, H.G. Im, Probabilistic approach to predict abnormal combustion in spark ignition engines, SAE paper (2018) 2018–01–1722.
[39] J. Zhang, M.B. Luong, F.E. Hernández Pérez, D. Han, H.G. Im, Z. Huang, Exergy loss of DME/air mixtures and ethanol/air mixtures with temperature and concentration fluctuations under HCCI/SCCI conditions: a DNS study, Combus. Flame 226 (2019) 334–346.
[40] M.B. Luong, S. Desai, F.E. Hernández Pérez, R. Sankaran, B. Johansson, H.G. Im, Effects of turbulence and temperature fluctuations on knock development in an ethanol/air mixture, Flow, Turbul. Combust. 106 (2021) 575–595.
[41] J.E. Dec, Advanced compression-ignition combustion for high efficiency and ultra-low NO_X and soot, in: T.K.D. Crolla, D.E. Foster, N. Vaughan (Eds.), Encyclopedia of Automotive Engineering, John Wiley & Sons, Ltd (2014), pp. 1–40.
[42] Y.-D. Liu, M. Jia, M.-Z. Xie, B. Pang, Enhancement on a skeletal kinetic model for primary reference fuel oxidation by using a semidecoupling methodology, Energy Fuels 26 (12) (2012) 7069–7083.
[43] P. Aleiferis, M. Behringer, J. Malcolm, Integral length scales and time scales of turbulence in an optical spark-ignition engine, Flow, Turbul. Combust. 98 (2) (2017) 523–577.
[44] M. Ivanov, V. Bychkov, et al., Turbulent flow produced by piston motion in a spark-ignition engine, Flow, Turbul. Combust. 82 (3) (2009) 317–337.
[45] B.R. Petersen, J.B. Ghandhi, High resolution scalar dissipation and turbulence length scale measurements in an internal combustion engine, SAE Int. J. Engines 3 (1) (2010) 65–83.
[46] G. Kalghatgi, Knock onset, knock intensity, superknock and preignition in spark ignition engines, Int. J. Engine Res. 19 (1) (2018) 7–20.
[47] S.L. Kokjohn, M.P. Musculus, R.D. Reitz, Evaluating temperature and fuel stratification for heat-release rate control in a reactivity-controlled compression-ignition engine using optical diagnostics and chemical kinetics modeling, Combust. Flame 162 (6) (2015) 2729–2742.
[48] S. Kaiser, M. Schild, C. Schulz, Thermal stratification in an internal combustion engine due to wall heat transfer measured by laser-induced fluorescence, Proc. Combust. Inst. 34 (2) (2013) 2911–2919.
[49] V. Akkerman, M. Ivanov, V. Bychkov, Turbulent flow produced by piston motion in a spark-ignition engine, Flow, Turbul. Combust. 82 (2009) 317–337.
[50] J.E. Dec, W. Hwang, Characterizing the development of thermal stratification in an HCCI engine using planar-imaging thermometry, SAE Trans. paper (2009) 2009–01–0650.
[51] L. Zhou, X. Zhang, L. Zhong, J. Yu, Effects of flame propagation velocity and turbulence intensity on end-gas auto-ignition in a spark ignition gasoline engine, Energies 13 (19) (2020) 5039.
[52] L. Chen, H. Wei, C. Chen, D. Feng, L. Zhou, J. Pan, Numerical investigations on the effects of turbulence intensity on knocking combustion in a downsized gasoline engine, Energy 166 (2019) 318–325.
[53] Z. Chen, Y. Ai, T. Qin, F. Luo, Quantitative evaluation of *n*-butane concentration on knock severity of a natural gas heavy-duty SI engine, Energy 189 (2019) 116244.